Dissociation Energies and Kinetics of Aminopyrimidinium Radicals by ab Initio and Density Functional Theory

František Tureček* and Jill K. Wolken

Department of Chemistry, Bagley Hall, Box 351700, University of Washington, Seattle, Washington 98195-1700

Received: December 30, 1998

A series of isomeric 4-aminopyrimidinium radicals were used to model hydrogen atom adducts of nucleobases containing the 4-aminopyrimidine structure motif. Relative stabilities and activation energies for dissociations by hydrogen atom loss have been calculated by density functional theory and ab initio methods up to effective QCISD(T)/6-311+G(2d,p) for 4-amino-N-1-H− (**1**), 2-H− (**2**), N-3-H− (**3**), 4-H− (**4**), 5-H− (**5**), and 6-H− (**6**) pyrimidinium radicals and the 4-pyrimidylammonium radical (**7**). All these radicals were found to be bound species existing in potential energy wells. The order of stabilities has been established as **5** (most stable) > **3** > **2** > **1** > **6** > **4** ≫ **7** (least stable). Dissociations of the N−H and C−H bonds in **1**-**7** required activation barriers above the dissociation thresholds. RRKM calculations of unimolecular rate constants for N−H bond dissociations in **1** and **3** predicted substantial stabilization of these radicals by kinetic shift in the gas phase. Additions of hydrogen atoms to the N-1, C-2, N-3, C-4, C-5, and C-6 ring positions in 4-aminopyrimidine were found to be exothermic by 68, 70, 76, 23, 91, and 62 kJ mol^{-1} at 0 K, respectively. Hydrogen atom addition to the NH_2 group was 58 kJ mol^{-1} endothermic. The activation barriers for the hydrogen atom additions to 4-aminopyrimidine were found to inversely correlate with the reaction enthalpies. The calculated rate constants predicted predominant (95%) hydrogen atom addition to C-5. The other positions were substantially less reactive, e.g., N-3 (2%), C-2 (1%), C-6 (0.8%), and N-1 (0.4%).

Introduction

Radical attacks on pyrimidine and purine nucleobases are considered to be one of the major chemical mechanisms of DNA damage.[1] When formed by radiolysis of water, the attacking species, OH• and H•, are presumed to add rapidly to nucleobase residues (N, Scheme 1).[2] In another mechanism of DNA damage,[3] electron capture by the nucleobase (N) is presumed to form an anion-radical (N•−) which is quenched by protonation in solution (Scheme 1). The resulting radical, (N + H)•, is formally analogous to the hydrogen atom adduct, but it may represent a different isomer.[1]

Early electron spin resonance (ESR) studies identified H-atom adducts to C-5 and oxygen atom upon irradiation of cytosine.[4,5] Similar results were obtained recently from heavy ion bombardment of nucleobases at low temperature.[6] Recently, Symons and co-workers studied cytosine and cytidine anion-radicals generated in liquid lithium chloride glasses.[7] On the basis of ESR spectra of deuterium-labeled derivatives, they concluded that protonation of anion-radicals occurred on the exocyclic amino group, yielding an unusual zwitterion.[7] These recent experimental results stressed the need for reliable relative energies of nucleobase radicals and activation energies for hydrogen atom additions.

The thermochemistry of OH• and H• adducts to nucleobases has been studied by Colson, Sevilla, and their co-workers for selected ring positions in adenine (C-4, C-5, and C-8), guanine (C-4, C-5, and C-8), cytosine (C-3, C-5, and C-6), and thymine (C-5 and C-6).[8−11] These authors used semiempirical and Hartree−Fock-level ab initio methods with small basis sets to evaluate isodesmic reactions for radical transfer between the nucleobase and a small organic radical.[10] The calculated C−H bond dissociation energies in the nucleobase radicals ranged between 79 and 134 kJ mol^{-1} depending on the nucleobase and the computational level used.[10] However, to our knowledge there have been no studies of the relative stabilities of H-atom adducts resulting from attacks at other ring positions in pyrimidine and purine derivatives and the activation energies for the H-atom additions.

SCHEME 1

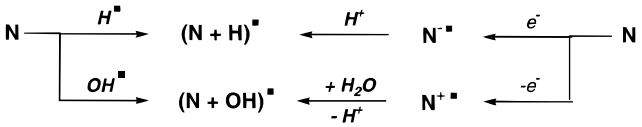

We have recently studied a model system, 4-aminopyrimidine, for which N−H radicals were generated in the gas phase by femtosecond electron transfer to stable aminopyrimidinium cations.[12] The 4-aminopyrimidinium radicals under study showed surprising stabilities in the gas phase, which were tentatively assigned to potential energy barriers to dissociations of N−H bonds. It was therefore of interest to compare the relative stabilities and dissociation energies of *a complete set* of 4-aminopyrimidinium radicals (**1**−**7**). These radicals can be viewed as simplified models[13] of cytosine and adenine radicals that incorporate the 4-aminopyrimidine structure motif. We now report a computational study that utilizes perturbational Moller−Plesset, quadratic configuration interaction, and density functional theory calculations with medium-size basis sets to provide relative stabilities for the isomeric radicals, bond dissociation energies, and activation energies for hydrogen atom additions. Rice−Ramsperger−Kassel−Marcus (RRKM) theory is used to calculate microcanonical rate constants for unimolecular radical dissociations. Transition state theory is used to calculate rate

10.1021/jp984826n CCC: $18.00
Published on Web 03/06/1999

constants for bimolecular addition of hydrogen atom to 4-aminopyrimidine. The energy data obtained for 4-aminopyrimidine will be used as a reference in a high-level computational study of cytosine radicals.[14]

Calculations

Standard ab initio calculations were carried out using the Gaussian 94 suite of programs.[15] Geometries were first optimized with Hartree−Fock calculations (RHF/6-31G(d,p) for molecules, UHF/6-31G(d,p) for radicals) and then re-optimized with density functional theory calculations using Becke's hybrid functional (B3LYP)[16,17] and the 6-31+G(d,p) basis set. Complete optimized structures, harmonic frequencies, and moments of inertia for **1**−**8** and transition states TS(**1**)−TS(**7**) are available as Supporting Information. B3LYP calculations have been reported to provide accurate optimized geometries for a number of systems,[18] and the 6-31+G(d,p) basis proved to be adequate for giving good quality radical geometries.[19] Harmonic frequencies were calculated with HF/6-31G(d,p) or B3LYP/6-31+G(d,p) and used to characterize local minima (all frequencies real) and first-order saddle points (1 imaginary frequency). Dissociation pathways were investigated with stepwise calculations in which the dissociating bond length was frozen while the remaining 32 degrees of freedom were fully optimized. The B3LYP frequencies were scaled by 0.961,[20−22] and the HF frequencies were scaled by 0.893[23] and used to calculate zero-point energy corrections, enthalpies, and partition functions. Single-point energies were obtained by B3LYP and Moller−Plesset perturbational calculations truncated at second order with frozen core excitations (MP2) using the larger 6-311G(2d,p) and 6-311+G(2d,p) basis sets. The spin-unrestricted MP2 calculations (UMP2) were affected by contamination from higher spin states that gave total spin values, $\langle S^2 \rangle = 1.1-1.2$. Annihilation of higher spin states by spin projection[24,25] reduced the $\langle S^2 \rangle$ values to 0.82−0.85 and resulted in projected MP2 energies (PMP2) that were lower by 20−28 mhartree. At the highest level of theory, quadratic configuration interaction calculations (QCISD(T))[26] were performed and extrapolated to effective QCISD(T)/6-311+G(2d,p) energies by a composite procedure (eq 1) based on the additivity approximation.[27]

$$\text{QCISD(T)/6-311+G(2d,p)} \approx \text{QCISD(T)/6-31G(d,p)} + \text{MP2/6-311+G(2d,p)} - \text{MP2/6-31G(d,p)} \quad (1)$$

This treatment is analogous to the G2(MP2) scheme[28] and its modifications[29−31] but uses smaller basis sets for the single-point calculations. The QCISD(T)/6-311+G(2d,p) energies were much less sensitive to spin contamination; the use of UMP2 or PMP2 energies in eq 1 resulted in differences in total energies that were <1 mhartree for radicals **1**−**7** and <3 mhartree for transition states.

RRKM calculations of unimolecular rate constants were performed using Hase's program.[32,33] Direct counting of quantum states was used to obtain microcanonical rate constants, *k(E,J,K)*, which were Boltzmann averaged over the rotational states to provide *k(E)* values. Bimolecular rate constants (mol^{-1} cm^3 s^{-1}) were calculated using the standard transition state theory formula.[34]

Results and Discussion

Radical Structures and Relative Stabilities. Geometry optimizations with B3LYP/6-31+G(d,p) gave local energy minima for radicals **1**−**7** and 4-aminopyrimidine (**8**) that were confirmed by harmonic frequency analyses. Structures **1**−**8** were rather unexceptional and thus deserve only a brief comment. Compared with **8**, radicals **1**−**6** showed longer bonds at the ring atoms carrying the additional hydrogen atom, e.g., N-1, C-2, N-3, C-4, C-5, and C-6 in **1**−**6**, respectively (Figure 1). The pyrimidine rings were only slightly puckered in **1**−**6**. For example, the N-1−H bond in **1** was deflected from the ring plane by 8.3°, whereas the N-3−H bond in **3** was pyramidized more substantially (30.5°, Figure 1). The latter effect may be due to steric interaction between the N-3−H and N-7−H-7a bonds, which causes out-of-plane deflection of both bonds. Radical **7** showed a long C-4−N-7 bond (Figure 1). In addition, the axial N-7−H-7c bond in the ammonium group was notably longer than the two equatorial N-7−H bonds (Figure 1).

The relative enthalpies of radicals **1**−**7** at 0 and 298 K are given in Table 1. At all levels of theory, radical **5** was the most stable isomer followed by **3**. Radicals **1**, **2**, and **6** had comparable relative enthalpies, whereas **4** and **7** were increasingly destabilized against **5**. In comparing the *relative stabilities*, the B3LYP and MP2 methods gave results that were in good agreement (±10 kJ mol^{-1}) with those from the higher level QCISD(T) calculations.

Radical Dissociations and Hydrogen Atom Additions. The calculated total energies of **1**−**7** and the energy of **8** allowed us to obtain the energies for hydrogen atom additions to **8** and for the reverse dissociations of the corresponding N−H and C−H bonds in the radicals. The data showed that the N−H and C−H bond dissociations were *endothermic* for all positions in **8** except the amino group (Table 2). Isomers **1**−**6** were therefore thermodynamically stable with respect to dissociations to **8** and a hydrogen atom, while isomer **7** was metastable. Compared with the QCISD(T) dissociation energies ($\Delta H^\circ_{r,298}$), the MP2 enthalpies were underestimated by 10−20 kJ mol^{-1}. This effect was most likely due to the imperfect correction of spin contamination in the MP2 calculations of the heterocyclic radicals.[12,35] By contrast, the B3LYP reaction enthalpies were uniformly overestimated by 10−20 kJ mol^{-1}. This systematic error was probably due to a better delocalization of valence electrons in **1**−**7**, as opposed to **8** + H$^\bullet$, which resulted in radical overstabilization.[36] Since the deviations in the MP2 and B3LYP dissociation energies consistently had a similar magnitude but opposite signs, very good agreement (±10 kJ mol^{-1}) with the QCISD(T) data was obtained by simple averaging of the PMP2 and B3LYP reaction enthalpies (Table 2). A similar empirical procedure has been recently reported to provide accurate proton affinities for a series of C_2H_6OS isomers.[37] This correction provides a convenient shortcut to good quality relative energies for heterocyclic radicals and allows one to circumvent the QCISD(T) calculations that are expensive for the systems under study and even more so for the larger nucleobase radicals.[14]

The reaction paths for dissociations of the pertinent N−H and C−H bonds in **1**−**7** were investigated by B3LYP/6-31+G(d,p) calculations that yielded transition state geometries and zero-point energies. Activation energies for unimolecular dissociations of **1**−**7** and the reverse hydrogen atom additions to **8** were obtained by single-point calculations, as summarized in Table 2. The calculated energies are related by eq 2, where BDE

$$\text{BDE(X−H)} = E_{\text{TS,dis}} - E_{\text{TS,add}} \quad (2)$$

is the dissociation energy of the X−H bond, $E_{\text{TS,dis}}$ is the activation energy for the bond dissociation, and $E_{\text{TS,add}}$ is the activation energy for hydrogen addition to the same position in **8**.

Dissociation of the N-1−H bond in **1** was calculated to require 40 kJ mol^{-1} above the thermochemical threshold defined by

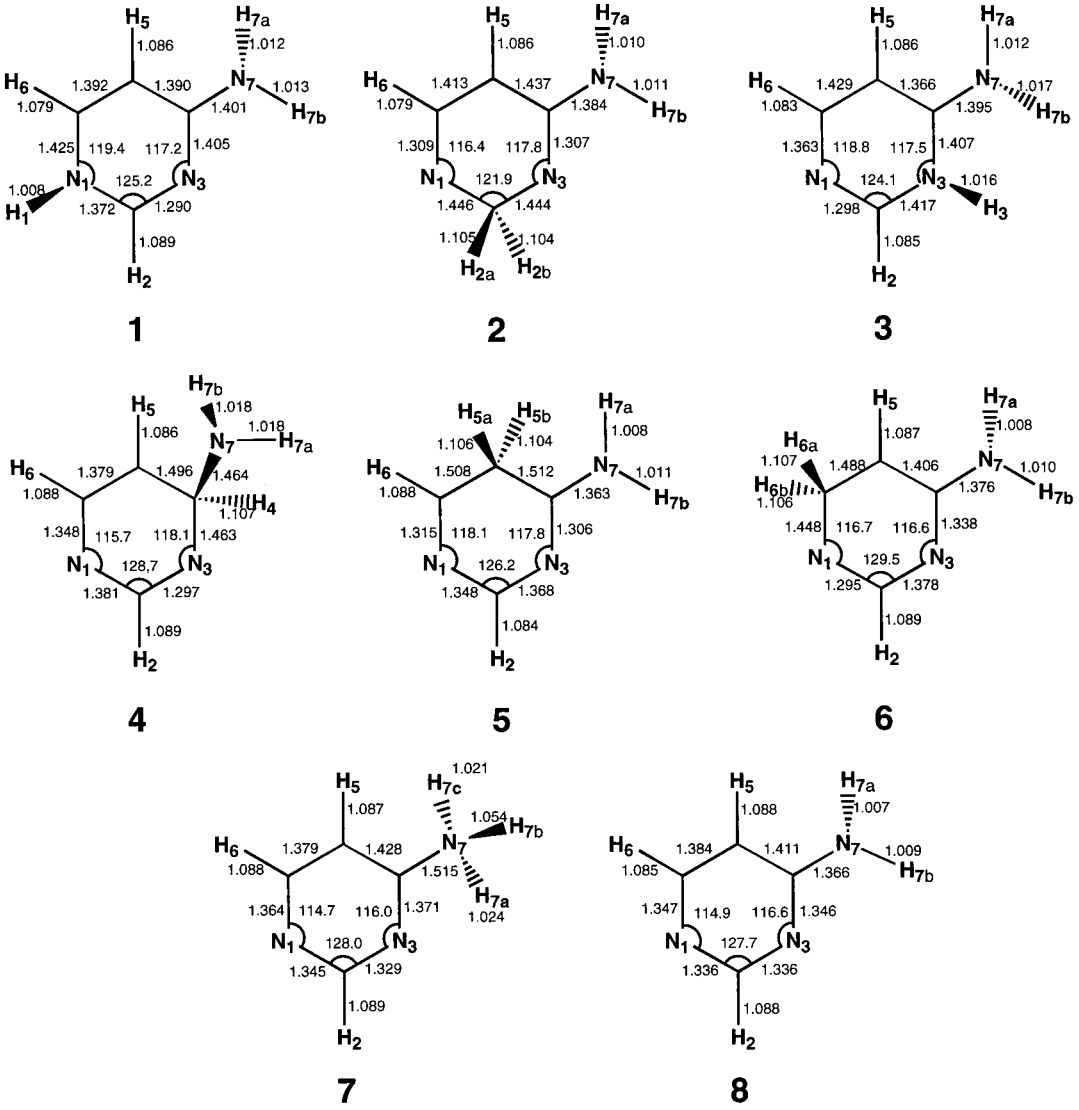

Figure 1. B3LYP/6-31+G(d,p) optimized geometries of radicals **1**−**7** and 4-aminopyrimidine (**8**).

TABLE 1: Relative Energies of Aminopyrimidinium Radicals 1−7

	relative energy[a]							
species	B3LYP/ 6-31+G(d,p)	B3LYP/6-311G(2d,p)		PMP2/ 6-311G(2d,p)	B3LYP/6-311+G(2d,p)		PMP2/ 6-311+G(2d,p)	QCISD(T) 6-311+G(2d,p)[b]
1	18.7	22.8	24.1[c]	25.3	15.1	18.6[c]	22.0	***23.4*** (25.2)[d]
2	24.4	24.5	25.1	25.7	23.6	24.3	25.0	***20.8*** (20.1)[d]
3	16.9	16.9	18.4	19.8	13.2	14.8	16.3	***15.0*** (14.5)[d]
4	79.4	79.8	78.1	76.4	78.9	77.8	76.7	***68.0*** (66.9)[d]
5	0	0	0	0	0	0	0	0 (0)[d]
6	29.6	29.4	32.5	35.5	28.6	31.7	34.8	***29.3*** (28.8)[d]
7	155.5	164.2	156.8	149.3	154.0	146.3	138.6	***149.4*** (147.5)[d]

[a] In kJ mol^{-1} at 0 K. [b] From eq 1. [c] Averaged MP2 and B3LYP energies. [d] 298 K values.

BDE(N-1−H) = 68 kJ mol^{-1}. The N-1−H bond was only partially interrupted in the transition state (r(N−H) = 1.602 Å), which indicated substantial interaction between the 1s semioccupied atomic orbital on the hydrogen atom and the frontier orbitals in **8**. Such an interaction is visualized by frontier orbital plots for **1**, TS(**1**), and **8** (Figure 2). The singly occupied molecular orbital (SOMO) in **1** is a π-type orbital. Since the H-1 atom lies close to the ring plane in **1**, the N-1−H bonding σ-orbital and SOMO are nearly orthogonal and do not mix constructively. In the transition state, the SOMO develops into a combination of the hydrogen s-type atomic orbital and a π-orbital resembling the HOMO in **8**. This requires changes in the nodal properties of the π-orbital components, e.g., along the C-2−N-3 and N-3−C-4 bonds and the dissociating N-1...H bond (Figure 2). The orbital analysis suggested that the reverse reaction, addition of H$^{\bullet}$ to **8**, must involve a three-electron, two-orbital interaction between the semioccupied 1s orbital on the hydrogen atom and the doubly occupied HOMO in **8**. In contrast, the LUMO in **8** was a diffuse orbital, which had negligible coefficients at N-1 and therefore could not overlap substantially with the 1s atomic orbital of the approaching hydrogen atom. The barrier for the hydrogen atom addition to N-1 in **8** is probably due to the reorganization energy required to redistribute the π electrons from the HOMO in **8** to another

TABLE 2: Reaction Enthalpies and Activation Energies for Dissociations of 1−7[a]

	relative energy[a]								
reaction	r(X−H)[b]	B3LYP/ 6-31+G(d,p)	B3LYP/6-311G(2d,p)		PMP2/ 6-311G(2d,p)	B3LYP/ 6-311+G(2d,p)		PMP2/ 6-311+G(2d,p)	QCISD(T)/ 6-311+G(2d,p)[c]
1 → **8** + H•		103.0	90.3	70.8[d]	51.4	95.7	73.1[d]	50.5	***67.6*** (69.6)[e]
1 → TS(**1**)	1.602	109.1	99.3	96.9	94.5	109.2	103.8	98.5	107.5
8 + H• → TS(**1**)		6.1	9.1	26.1	43.1	13.5	30.8	48.0	39.9
2 → **8** + H•		97.3	88.5	69.7	51.0	87.2	67.3	47.5	***70.1*** (74.6)[e]
2 → TS(**2**)	1.845	107.7	104.6	94.7	84.9	106.0	95.6	85.2	107.0
8 + H• → TS(**2**)		10.4	16.1	25.0	33.9	18.9	28.3	37.7	36.9
3 → **8** + H•		104.9	96.1	76.6	57.0	97.6	76.9	56.1	***76.0*** (80.2)[e]
3 → TS(**3**)	1.638	109.0	103.5	99.9	96.2	109.3	104.6	100.0	111.2
8 + H• → TS(**3**)		4.1	7.3	23.3	39.3	11.7	27.8	43.8	35.2
4 → **8** + H•		42.4	33.2	16.7	0.3	31.9	13.9	−4.2	***23.0*** (27.8)[e]
4 → TS(**4**)	1.666	76.5	73.7	69.1	64.6	74.3	69.2	64.0	86.3
8 + H• → TS(**4**)		34.1	40.5	52.4	64.3	42.4	55.3	68.2	63.4
5 → **8** + H•		121.7	113.0	94.9	76.7	110.8	91.6	72.5	***91.0*** (94.7)[e]
5 → TS(**5**)	1.979	123.1	118.6	109.8	101.1	120.5	111.1	101.6	117.5
8 + H• → TS(**5**)		1.3	5.5	14.9	24.4	9.7	19.4	29.1	26.5
6 → **8** + H•		74.1	65.7	44.5	23.3	64.2	41.9	19.7	***61.7*** (66.0)[e]
6 → TS(**6**)	1.840	85.4	82.3	70.5	58.7	83.8	71.5	59.2	100.1
8 + H• → TS(**6**)		11.2	16.6	26.0	35.4	19.6	29.6	39.5	38.4
7 → **8** + H•		−33.7	−51.2	−61.9	−72.6	-43.2	-54.7	-66.1	−***58.4*** (−54.1)[e]
7 → TS(**7**)	1.350	2.6	−8.2	5.5	19.2	2.0	14.8	27.6	21.7
8 + H• → TS(**7**)		36.3	43.0	67.4	91.8	45.2	69.5	93.7	80.0

[a] 0 K values in kJ mol^{-1}. [b] Dissociating bond lengths (Å) in transition states. [c] Effective energies from eq 1. [d] Averaged B3LYP and PMP2 energies. [e] 298 K values.

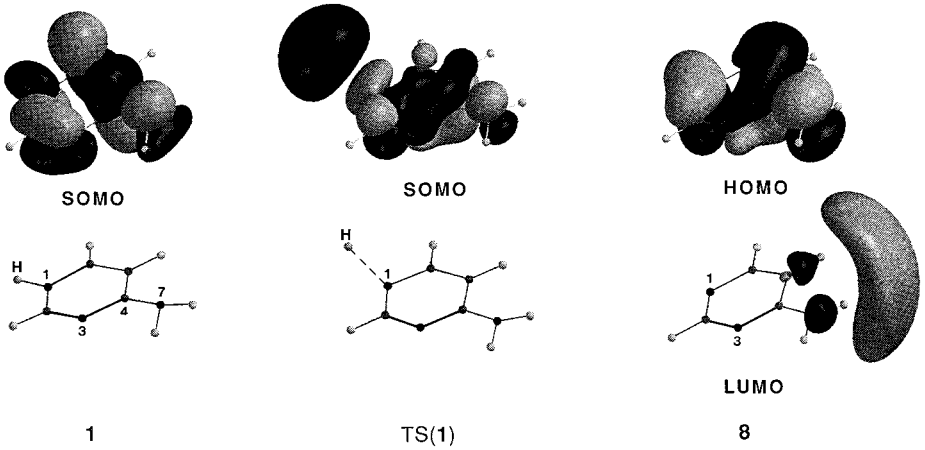

Figure 2. Frontier orbitals in **1**, TS(**1**), and **8** from HF/6-311+G(2d,p) wave functions.

orbital in the transition state. Note that this orbital interaction differs from that for the analogous addition of a hydrogen atom to the nitrogen atom in pyridine, which involved a conventional H(1s)-LUMO mixing in the transition state.[13]

Dissociation of the N-3−H bond in **3** was in all respects similar to that of the N-1−H bond. The transition state was found at r(N−H) = 1.638 Å, which required 35 kJ mol^{-1} above the thermochemical threshold given by the BDE(N-3−H) = 76 kJ mol^{-1} at 0 K (Table 3). The frontier orbital interactions in the dissociation of the N-3−H bond in **3** are shown in Figure 3. In the transition state, the π-type SOMO in **3** develops into a combination of a hydrogen atom s-type orbital and the HOMO in **8** (the latter orbital is depicted with an inverted phase). Hence, addition of the hydrogen atom to N-3 in **8** involves a three-electron two-orbital interaction resulting in reorganization of the HOMO π-electrons.

Dissociation of the N-7−H bond in **7** was different. Radical **7** was a highly polarized species, which can be represented by a zwitterionic structure consisting of a pyrimidine anion-radical and the positively charged ammonium group.[7,12] Accordingly, the SOMO in **7** was a π orbital that was delocalized in the pyrimidine ring. Dissociation of the axial N-7−H bond required only 22 kJ mol^{-1} above **7** and was accompanied by continuous reorganization of the SOMO, which retained its nodal properties in the transition state (Figure 4). The reverse addition of a hydrogen atom to the amino group in **8** was 58 kJ mol^{-1} endothermic and had to overcome an activation barrier of 80 kJ mol^{-1}. This activation energy is probably due to the substantial electron reorganization during the first phase of the addition, when the electron density is forced to flow from the amino group into the pyrimidine ring.

Dissociation of the most stable radical **5** showed a potential energy profile continuously increasing along the C-5−H coordinate up to r(C-5−H) = 1.979 Å, where a transition state was located (Figure 5). The activation energy for a hydrogen atom addition to C-5 in **8** was calculated by QCISD(T)/6-311+G(2d,p) at 26.5 kJ mol^{-1}, which was the lowest value for any position in **8**. Hence, radical **5** is both thermodynamically and kinetically the most stable isomer, which should be formed preferentially upon hydrogen atom addition to **8**.

Dissociations of the C-2−H bond in **2** and the C-6−H bond in **6** showed rather similar characteristics (Table 3). Transition states were found at C−H bond lengths of 1.845 and 1.85 Å, respectively. The transition states for the dissociations of **2** and

TABLE 3: Ab Initio Calculated Arrhenius Parameters for Dissociations of Aminopyrimidinium Radicals and Addition of Hydrogen Atoms to 4-Aminopyrimidine

reaction	E_0	E_a[a]	log A	r^2	$k_{i,298}$[b]	$100k_i/\sum k_i$
			QCISD(T)/6-311 + G(2d,p) Energies			
1 → **8** + H•	107.47	105.81	11.83	0.9997_9	2.2×10^{-7}	
8 + H• → **1**	39.88	37.22	12.41	0.9999_9	7.8×10^{5}	0.4
2 → **8** + H•	107.04	110.31	13.33	0.9999_9	9.4×10^{-7}	
8 + H• → **2**	36.89	34.07	12.37	0.9999_8	2.5×10^{6}	1.4
3 → **8** + H•	111.20	113.51	13.10	0.9999_9	1.6×10^{-7}	
8 + H• → **3**	35.22	35.93	12.92	0.9998_6	4.0×10^{6}	2.2
4 → **8** + H•	86.34	88.74	12.95	0.9999_7	2.4×10^{-3}	
8 + H• → **4**	63.38	59.29	11.97	0.9999_8	4.0×10^{2}	0.0
5 → **8** + H•	117.52	120.08	12.70	0.9999_9	1.1×10^{-9}	
8 + H• → **5**	26.53	23.82	12.41	0.9999_8	1.7×10^{8}	95.2
6 → **8** + H•	100.08	103.20	13.29	0.9999_7	1.5×10^{-5}	
8 + H• → **6**	38.42	35.71	12.41	0.9999_9	1.4×10^{6}	0.8
7 → **8** + H•	21.66	23.29	12.85	0.9998_6	5.7×10^{8}	
8 + H• → **7**	80.02	72.73	13.03	0.9998_6	5.2×10^{-2}	0.0
			Averaged PMP2 + B3LYP/6-311 + G(2d,p) Energies			
1 → **8** + H•	103.84	104.49	12.30	0.9997_9	9.7×10^{-7}	
8 + H• → **1**	30.75	28.09	12.41	0.9999_9	3.1×10^{7}	1.0 (1.0)[c]
2 → **8** + H•	95.6	98.89	13.32	0.9999_9	9.4×10^{-5}	
8 + H• → **2**	28.3	25.47	12.37	0.9999_7	8.1×10^{8}	2.5 (1.5)
3 → **8** + H•	105.83	108.13	13.10	0.9999_9	1.4×10^{-6}	
8 + H• → **3**	28.94	29.65	12.92	0.9998_6	5.0×10^{7}	1.5 (2.5)
4 → **8** + H•	69.17	71.57	12.95	0.9999_5	1.0×10^{3}	
8 + H• → **4**	55.31	51.22	11.97	0.9999_7	2.5	0.0 (0.0)
5 → **8** + H•	111.07	113.63	12.70	0.9999_8	5.9×10^{-8}	
8 + H• → **5**	19.44	16.73	12.41	0.9999_8	3.0×10^{9}	93.4 (93.9)
6 → **8** + H•	71.5	74.6	13.29	0.9999_5	1.6	
8 + H• → **6**	29.6	26.8	12.41	0.9999_9	5.2×10^{7}	1.6 (1.1)
7 → **8** + H•	14.83	16.43	12.85	0.9998_6	9.0×10^{9}	
8 + H• → **7**	69.47	64.90	11.91	0.9998_6	3.7	0.0 (0.0)

[a] Arrhenius activation energy in kJ mol^{-1}. [b] Bimolecular rate constants in mol^{-1} cm^3 s^{-1}, unimolecular rate constants in s^{-1}. [c] Values in parentheses are from the averaged PMP2 and B3LYP/6-311G(2d,p) calculations.

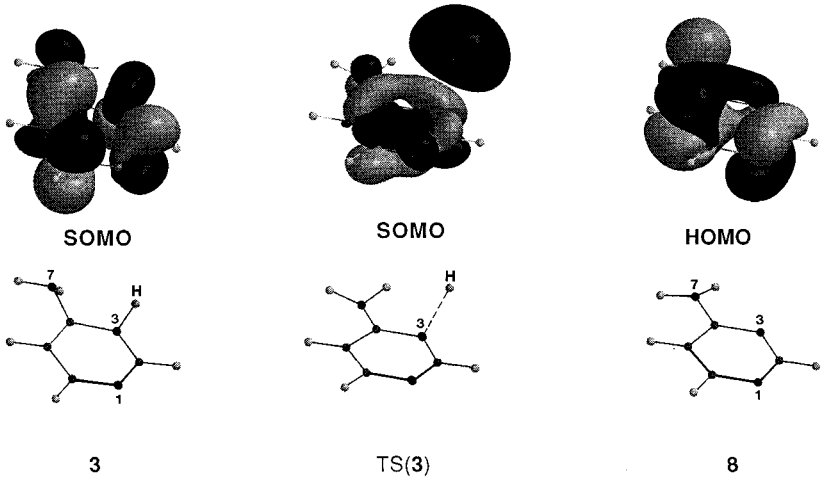

Figure 3. Frontier orbitals in **3**, TS(**3**), and **8** from HF/6-311+G(2d,p) wave functions.

6 were obtained with similar energies as were the activation energies for additions of hydrogen atoms to C-2 and C-6, 37 and 38 kJ mol^{-1}, respectively (Table 3).

The C-4−H bond in **4** was weak, BDE(C-4−H) = 23 kJ mol^{-1} at 0 K. Interestingly, the dissociation of the C-4−H bond was found to require 63 kJ mol^{-1} above the thermochemical threshold. Radical **4** was therefore kinetically stabilized against dissociation. However, addition of a hydrogen atom to C-4 in **8** is hampered by the presence of the large activation barrier.

Dissociation and Hydrogen Addition Kinetics. Having characterized the transition states for hydrogen loss and addition, we have calculated the rate constants for these reactions. Unimolecular rate constants for dissociations of the N−H bonds in **1**, **3**, and **7** were relevant to the experimentally observed stability of 4-aminopyrimidinium radicals in the gas phase.[12] The RRKM rate constants are shown in Figure 6 as plots of log k_{uni} versus internal energy. Radical **3** had a slightly higher activation energy for H loss (111.2 kJ mol^{-1}) than did radical **1** (107.5 kJ mol^{-1}). However, the log k_{uni} curves crossed at ~5 kJ mol^{-1} above TS(**1**) such that the N-3−H bond dissociation in **3** was faster than the dissociation of the N-1−H bond in **1** over a broad range of internal energies (Figure 6a). Both log k_{uni} curves showed a shallow rise with the radical internal energy. For the experimental time scale of 4.7 μs,[12] the half-lives for the dissociations appeared at log k_{uni} = 5.17. Figure 6a shows that achieving this rate constant was accompanied by substantial kinetic shifts, ΔE = 32 and 22 kJ mol^{-1} for **1** and **3**, respectively. By contrast, dissociation of the N-7−H bond

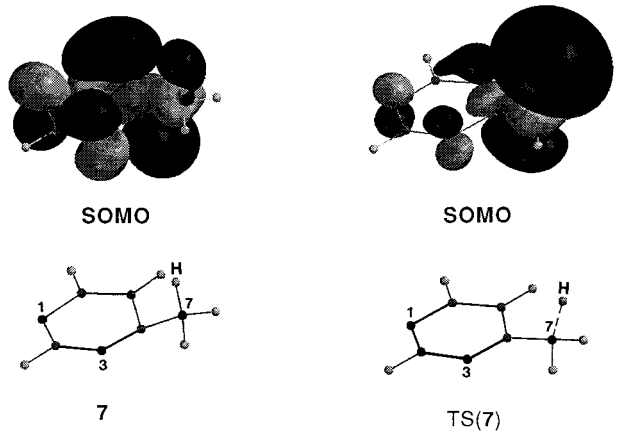

Figure 4. Frontier orbitals in **7** and TS(**7**) from HF/6-311+G(2d,p) wave functions.

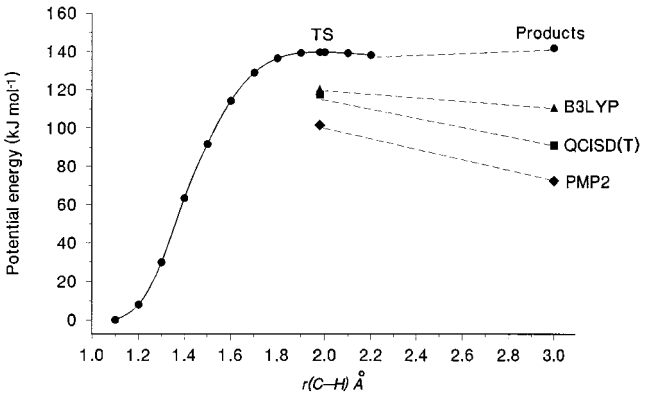

Figure 5. B3LYP/6-31+G(d,p) potential energy profile for the dissociation of the C-5−H bond in **5**. Circles: B3LYP/6-31+G(d,p) energies. Triangles: B3LYP/6-311+G(2d,p) energies with ZPVE corrections. Squares: Effective QCISD(T)/6-311+G(2d,p) energies with ZPVE corrections. Diamonds: PMP2/6-311+G(2d,p) energies with ZPVE corrections.

in **7** showed a steeply rising log k_{uni} curve (Figure 6b), which reached log $k_{uni} = 8$ within 1 kJ mol^{-1} above the transition state energy. These calculations indicated that radicals **1** and **3** were kinetically stabilized against dissociation to **8** and a hydrogen atom in the gas phase. Radical **7** was predicted to be unstable on the microsecond time scale and should be difficult if not impossible to prepare by collisional electron transfer. The facile dissociation of **7** is in an apparent contradiction with the results of Symons, who reported a stable cytosine radical analogous to **7**.[7] However, it is possible that the highly polar cytosine radical was stabilized by the ionic medium or polar solvent used in the trapping experiments.[7]

Additions of hydrogen atoms to **8** can yield isomers **1**−**6** by exothermic reactions. The kinetics of the hydrogen atom additions were therefore of interest for establishing the product distribution in this model system. The rate constants for bimolecular reactions of **8** with H$^{\bullet}$, k_{bimol}, were calculated from the transition state theory formula (eq 3),[34,38] where k_B is the Boltzmann constant, N_A is the Avogadro number, h is the Planck constant, V_m is the molar volume, T is the absolute temperature, and R is the gas constant.

$$k_{bimol} = \frac{k_B T N_A V_m}{b} \frac{Q_{TS}}{Q_H Q(\mathbf{8})} e^{-E_0/RT} \qquad (3)$$

The E_0 values were obtained from QCISD(T)/6-311+G(2d,p) transition state energies and B3LYP/6-31+G(d,p) zero-point

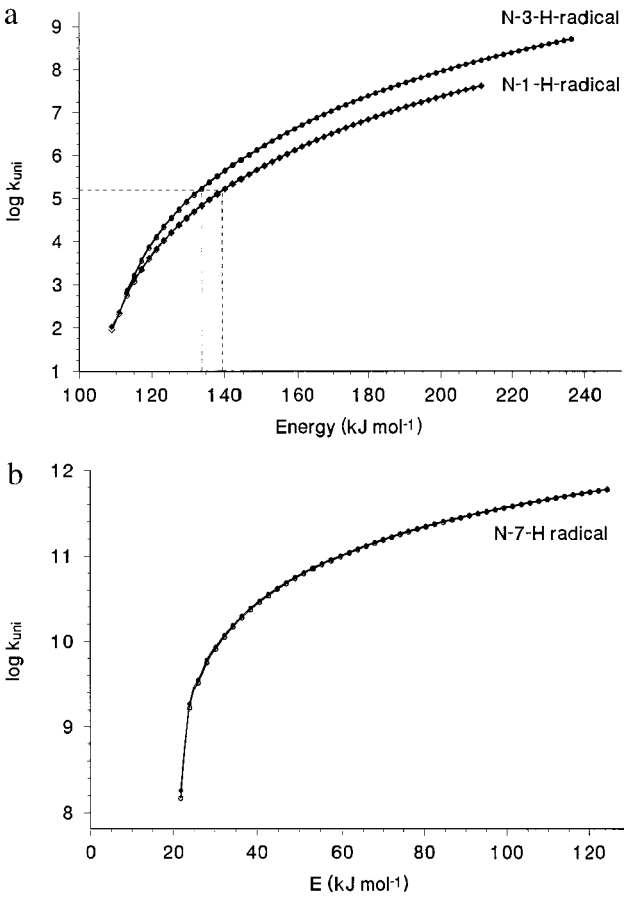

Figure 6. RRKM unimolecular rate constants for N−H bond dissociations in (a) **1** and **3** and (b) **7**. k_{uni} were calculated for $T_{rot} = 423$ and 523 K. The broken lines show the region of experimental kinetic stability for **1** and **3**.

corrections. The partition functions, $Q = Q_{el}Q_{trans}Q_{rot}Q_{vib}$, for the reactants and transition states were obtained from the calculated (scaled) harmonic frequencies (for Q_{vib}) and moments of inertia (for Q_{rot}), using standard thermodynamic formulas.[38] Rate constants for unimolecular dissociations of thermal radicals **1**−**7**, k_{unimol} were treated analogously.

Plotting the calculated log k values against $1/T$ in the range of $T = 200$−550 K showed very good Arrhenius behavior with correlation coefficients $r^2 = 0.999$ or better. The fitted Arrhenius activation energies (E_a) and preexponential factors (log A) are summarized in Table 3. The E_a and log A were calculated to give k_{bimol} in units of mol^{-1} cm^3 s^{-1} and k_{unimol} in s^{-1}. The absolute rate constants for hydrogen atom additions to **8** differed by 2−3 orders of magnitude when calculated at the different levels of theory. However, the *relative values*, $k_i/\sum k_i$, were similar (Table 3). Since the relative rate constants are equal to the relative rates of hydrogen atom addition to the different sites in **8**, the calculated $k_i/\sum k_i$ values were used to predict the site selectivities. Both the QCISD(T) and the averaged (MP2 + B3LYP) calculations predicted predominant addition to C-5 in **8**, 93−95% (Table 3). The other sites were much less reactive, e.g., N-3 (2%), C-2 (1−2%), N-1 (∼1%), and C-6 (∼1%). C-4 and the amino group were unreactive.

The calculated relative rate constants showed that the averaged PMP2 and B3LYP calculations performed very well compared with the much more expensive effective QCISD(T) method. This finding is significant for the calculations of radicals derived from larger systems, e.g., adenine, guanine, cytosine, uracil, and thymine, for which QCISD(T) calculations may not be feasible even with the moderate 6-31G(d,p) basis set.[14]

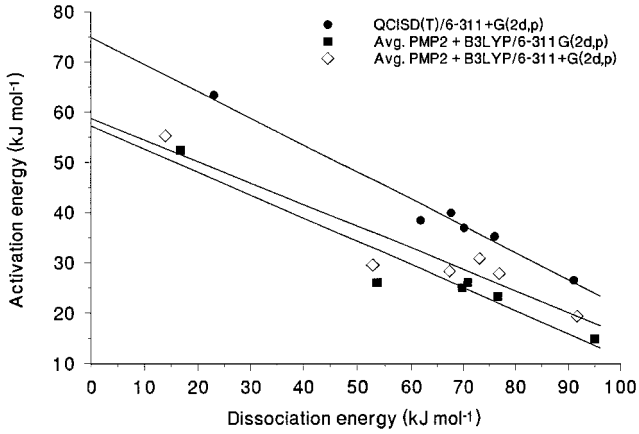

Figure 7. Correlation between the energy barriers for hydrogen atom additions and the reaction exothermicities.

Nevertheless, investigations of potential energy surfaces in radicals were tedious even in **1**−**7**. In nucleobases, the large number of tautomers and radicals derived therefrom presents a daunting task for selecting the kinetically relevant transition states. We found empirically that for **1**−**7** the energy barriers (E_0) for the hydrogen atom additions correlated with the reaction exothermicities ($-\Delta H_{add}$) according to eq 4.

$$E_0 = -a\Delta H_{add} + c \qquad (4)$$

The correlations are shown for **1**−**6** in Figure 7 for the effective QCISD(T)/6-311+G(2d,p) and averaged PMP2 and B3LYP energies. Since hydrogen atom addition to the NH_2 group in **8** was 80 kJ mol^{-1} endothermic and therefore negligibly slow at any relevant temperature, isomer **7** was omitted from the correlations. The QCISD(T) data showed the best fit (a = 0.5365, c = 74.9, r^2 = 0.9799, s(E) = 2.0 kJ mol^{-1}). Those for the averaged PMP2 and B3LYP calculations were less tight, e.g., a = 0.4598 and 0.4295, c = 57.2 and 58.7, r^2 = 0.929 and 0.908, s(E) = 3.8 and 4.1 kJ mol^{-1}, for the 6-311G(2d,p) and 6-311+G(2d,p) basis sets, respectively. The regressions showed very good estimates for the lowest activation energies for the hydrogen atom addition to C-5 (ΔE < 1.3 kJ mol^{-1}).

Empirical correlations between E_0 and ΔH_r have been introduced by Evans and Polanyi for reactions of alkali metal atoms with alkyl halides[39,40] and used for other systems as well.[41] In the present case of hydrogen atom additions to **8**, the ΔH_{add} values follow the order of radical stabilities, $\Delta H_{add} = -\Delta H_{dis}$. This may have practical ramifications for predicting the order of activation energies for hydrogen atom additions to nucleobases based on the calculated relative stabilities of nucleobase radicals.[10,14] The latter values are much easier to calculate than the potential energy barriers.

A qualitative relationship was also sought between the activation energies for H-atom additions and the calculated atomic charges in **8** (Figure 8), as discussed previously for nucleobases.[2,11] C-5 had the highest electron density of the ring carbon atoms, corresponding to its highest affinity for the hydrogen atom. However, the much more electronegative nitrogen atoms in **8** showed lower hydrogen atom affinities and higher activation energies than did C-5. It appears that the nodal properties of the frontier orbitals in **8** are the primary determinant affecting the activation energies for H-atom additions.

Conclusion

Radicals produced by hydrogen atom additions to 4-aminopyrimidine (**8**) were stable species. Effective QCISD(T)/6-311+G(2d,p) calculations predicted C-5 to be the preferred site of H atom attack to give rise to the most stable 4-amino-5(*H*)-pyrimidinium radical. Additions to all ring positions in **8** were exothermic. Addition to the amino group was endothermic. PMP2 and B3LYP calculations showed systematic errors of similar magnitude but opposite signs. Averaged PMP2 and B3LYP energies gave reaction enthalpies and activation energies that agreed well with the QCISD(T) data. The calculated activation energies for H atom additions to **8** correlated with the reaction exothermicities. The use of inexpensive MP2 and B3LYP computations and the empirical correlations between the radical stabilities and activation energies are promising for predicting the reactivity of heteroaromatic molecules and nucleobases in radical additions.

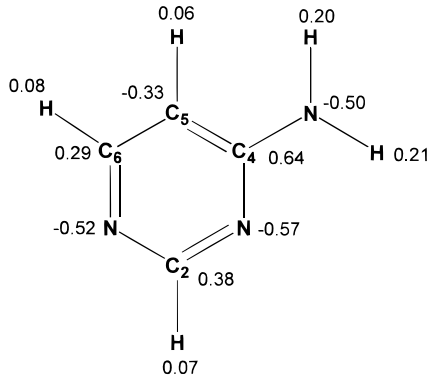

Figure 8. Total atomic charges in **8** from Mulliken population analysis with the 6-311G(2d,p) basis set.

Acknowledgment. Support of this work by the National Science Foundation (Grant CHE-9712570), the University of Washington Faculty Workstation Initiative, and Selectide, Inc., is gratefully acknowledged. We thank Dr. David Hrovat for invaluable help with computations and data visualization.

Supporting Information Available: Tables of B3LYP/6-31+G(d,p) optimized geometries and harmonic frequencies. This information is available free of charge via the Internet at http://pubs.acs.org.

References and Notes

(1) von Sonntag, C. In *Physical and Chemical Mechanisms in Molecular Radiation Biology*; Glass, W. A., Varma, M. N., Eds.; Plenum Press: New York, 1991; pp 287−321.
(2) Steenken, S. *Chem. Rev.* **1989**, *89*, 503.
(3) Symons, M. C. R. *J. Chem. Soc., Faraday Trans. 1* **1987**, *83*, 1.
(4) Westhof, E.; Flossmann, W.; Muller, A. *Int. J. Radiat. Biol.* **1975**, *28*, 427.
(5) Flossmann, W.; Westhof, E.; Muller, A. *J. Chem. Phys.* **1976**, *64*, 1688.
(6) Schaefer, A.; Huttermann, J.; Kraft, G. *Int. J. Radiat. Biol.* **1993**, *63*, 139.
(7) Cullis, P. M.; Malone, M. E.; Podmore, I. D.; Symons, M. C. R. *J. Phys. Chem.* **1995**, *99*, 9293.
(8) Colson, A.-O.; Sevilla, M. D. *J. Phys. Chem.* **1995**, *99*, 13033.
(9) Colson, A.-O.; Sevilla, M. D. *J. Phys. Chem.* **1996**, *100*, 4420.
(10) Colson, A.-O.; Becker, D.; Eliezer, I.; Sevilla, M. D. *J. Phys. Chem. A* **1997**, *101*, 8935.
(11) For a review of previous computational work see: Colson, A.-O.; Sevilla, M. D. *Int. J. Radiat. Biol.* **1995**, *67*, 627.
(12) Nguyen, V. Q.; Turecek, F. *J. Am. Chem. Soc.* **1997**, *119*, 2280.
(13) Turecek, F. *J. Mass Spectrom.* **1998**, *33*, 779.
(14) Wolken, J. K.; Turecek, F. Unpublished results.
(15) *Gaussian 94* (Revision E.3); M. J. Frisch, G. W. Trucks, H. B. Schlegel, P. M. W. Gill, B. G. Johnson, M. A. Robb, J. R. Cheeseman, T. Keith, G. A. Petersson, J. A. Montgomery, K. Raghavachari, M. A. Al-Laham, V. G. Zakrzewski, J. V. Ortiz, J. B. Foresman, J. Cioslowski, B. B. Stefanov, A. Nanayakkara, M. Challacombe, C. Y. Peng, P. Y. Ayala, W. Chen, M. W. Wong, J. L. Andres, E. S. Replogle, R. Gomperts, R. L.

Martin, D. J. Fox, J. S. Binkley, D. J. Defrees, J. Baker, J. P. Stewart, M. Head-Gordon, C. Gonzalez, and J. A. Pople; Gaussian, Inc.: Pittsburgh, PA, 1995.

(16) Becke, A. D. *J. Chem. Phys.* **1993**, *98*, 1372, 5648.

(17) Stephens, P. J.; Devlin, F. J.; Chablowski, C. F.; Frisch, M. J. *J. Phys. Chem.* **1994**, *98*, 11623.

(18) Bauschlicher, C. W.; Partridge, H. *J. Chem. Phys.* **1995**, *103*, 1788.

(19) Frank, A. J.; Sadilek, M.; Ferrier, J. G.; Turecek, F. *J. Am. Chem. Soc.* **1997**, *119*, 12343.

(20) Rauhut, G.; Pulay, R. *J. Phys. Chem.* **1995**, *99*, 3093.

(21) Finley, J. W.; Stephens, P. J. *J. Mol. Struct. (THEOCHEM)*, **1995**, *357*, 225.

(22) Wong, M. W. *Chem. Phys. Lett.* **1996**, *256*, 391.

(23) Hehre, W. J.; Radom, L.; Schleyer, P. v. R.; Pople, J. A. *Ab Initio Molecular Orbital Theory*; Wiley: New York, 1986; pp 228−236.

(24) Mayer, I. *Adv. Quantum Chem.* **1980**, *12*, 189.

(25) Schlegel, H. B. *J. Chem. Phys.* **1986**, *84*, 4530.

(26) Pople, J. A.; Head-Gordon, M.; Raghavachari, K. *J. Chem. Phys.* **1987**, *87*, 5968.

(27) Nobes, R. H.; Bouma, W. J.; Radom, L. *Chem. Phys. Lett.* **1982**, *89*, 497.

(28) Curtiss, L. A.; Raghavachari, K.; Trucks, G. W.; Pople, J. A. *J. Chem. Phys.* **1991**, *94*, 7221.

(29) Raghavachari, K.; Stefanov, B. B.; Curtiss, L. A. *J. Chem. Phys.* **1997**, *106*, 6764.

(30) Curtiss, L. A.; Redfern, P. C.; Smith, B. J.; Radom, L. *J. Chem. Phys.* **1996**, *104*, 5148.

(31) Smith, B. J.; Radom, L. *J. Phys. Chem.* **1995**, *99*, 6468.

(32) Zhu, L.; Hase, W. L. *Quantum Chemistry Program Exchange*; Indiana University: Bloomington, IN, 1994; Progam No. QCPE 644.

(33) Zhu, L.; Hase, W. L. *Chem. Phys. Lett.* **1990**, *175*, 117.

(34) Laidler, K. J.; Polanyi, J. C. In *Progress in Reaction Kinetics*; Porter, G., Ed.; Pergamon: Oxford, U.K., 1965; Vol. 3, pp 3−61.

(35) Nguyen, V. Q.; Turecek, F. *J. Mass Spectrom.* **1997**, *32*, 55.

(36) For another example of radical overstabilization by DFT methods see: Nguyen, M. T.; Creve, S.; Vanquickenborne, L. G. *J. Phys. Chem.* **1996**, *100*, 18422 and references therein.

(37) Turecek, F. *J. Phys. Chem. A* **1998**, *102*, 4703.

(38) Levine, I. N. *Physical Chemistry*, 3rd ed.; McGraw-Hill: New York, 1988; pp 783−796.

(39) Evans, M. G.; Polanyi, M. *Trans. Faraday Soc.* **1938**, *34*, 11.

(40) Butler, E. T.; Polanyi, M. *Trans. Faraday Soc.* **1943**, *39*, 19.

(41) Donahue, N. M.; Clarke, J. S.; Anderson, J. G. *J. Phys. Chem. A* **1998**, *102*, 3923 and references therein.